COMPUTATIONAL AND EXPERIMENTAL DEVELOPMENT OF NOVEL HIGH TEMPERATURE ALLOYS

Matthew J Kramer, Travis Brammer, Kevin Severs, Pratik K. Ray and Mufit Akinc
Ames Laboratory and the Department of Materials Science and Engineering
Iowa State University, Ames, IA 50011

ABSTRACT

We are continuing our efforts in proof-of-concept of a new high temperature alloy based on our previous efforts on computational materials discovery. The architectural framework for our material's design is a refractory base metal with a high temperature intermetallic which provides both high temperature strength and a source of oxidatively stable elements. Mo has been selected as the best candidate as the refractory backbone metal. For Fossil applications, Ni-Al appears to be the best choice to provide the source of oxidatively stable elements but this system requires a 'boost' in melting temperatures to be viable candidate in the ultra-high temperature regime (> 1200°C). Efforts have been in two areas, optimization of the Mo content in the base metal and refinement of the Ni-Al outer coating chemistry for oxidation stability. We have demonstrated that the base ternary alloy can be directionally solidified to form a well aligned dendritic structure with Mo content around 20 at. %. Higher content seems possible but beyond our present capability at this point. We believe to have identified the effect of the noble elements on increasing oxidation stability. A model for predicting the oxidation of the ternary alloy has been developed. Oxidation pathways and isothermal and cyclic oxidation results will be presented for temperatures up to 1200°C and 10 hrs.

INTRODUCTION

Superalloys have long been considered as the materials for choice in harsh environments[1]. While the actual materials have components melting around 1250°C [1], application thermal barrier coatings can certainly boost the operating temperatures. However, in boosting the operating temperatures, almost 30% of the energy input gets used up for the purpose of cooling, thereby affecting the overall efficiency adversely. Therefore, there is an urgent need for developing alloys that have high melting temperature and high temperature environmental resistance. In this article, we report a multi-stage hierarchical sieving approach to alloy design.

In this approach, the first step involves the use of semi-empirical models as the first stage of screening potential alloy systems. It has been shown that cohesive energy plays an important role in the melting temperature of materials[2]. This concept has been used to calculate the melting temperatures of binary alloys as well[3]. In order to determine the cohesive energy of the compound, it is essential to the formation enthalpy as well. This was estimated using an extended Miedema model[4]. In addition to having a high melting temperature, the target alloy should also have good high temperature mechanical properties and oxidation resistance. Based on these criteria, the base alloy system was selected to be Mo-Ni-Al with a Mo+NiAl two-phase field.

The second step involved boosting the melting temperatures of the NiAl beyond 1638°C. These were done by controlled additions of platinum group metals (PGMs). Ideally, the additions should reduce the formation enthalpy in order to increase the melting temperatures. These additions were identified after doing *ab-initio* studies using the VASP software. The results from these studies have been described elsewhere[5]. The third step was to carry out the oxidation tests on these alloys, with the final step being packaging the two phases effectively.

THEORETICAL CALCULATIONS

A simplified 2D probabilistic Cellular Automata model, with the following set of assumptions, were used for the preliminary calculations –

a) Mo reacts with oxygen to form MoO_3, which volatilizes leaving the space exposed to fresh oxygen from the air.
b) If NiAl surface gets exposed due to volatilization of MoO_3, Al_2O_3 forms and seals the surface from further oxidation.
c) Al_2O_3, once formed, does not spall.
d) A 2D picture can represent the alloy cross-section and oxidation behavior does not vary across different sections perpendicular to the coupon surface.
e) Each grid in the lattice depicting the microstructure represents a single grain. Periodic boundary conditions are assumed at the vertical edges of the cell.
f) Oxygen present in a given grid can penetrate a maximum of one grain diameter in any direction in a single time-step.

A microstructure was created using random numbers generated by the computer code. The computer clock was used to seed the random sequence, which otherwise would have been a pseudo-random sequence with same numbers being generated for every run under identical conditions. The upper bound of the random sequence was set to 100. For each grid in the microstructure, a random number was generated; if the number was below the Molybdenum composition expressed as a percentage, the grid was assigned a number value corresponding to the Mo and NiAl respectively. The computation was performed on a 150 x 150 square lattice. Two lists were created, one of which stored the location of the oxygen, while the other contained a description (in terms of the assigned number value) of the different phases. The calculations were carried out assuming a Von Neumann neighborhood, with only the edge sharing neighboring cells being considered. Each oxidation step consisted of scanning the neighborhood around the oxygen cells, with the appropriate oxidation steps being carried out. In event of the oxygen cell being adjacent to both NiAl and Mo cells, Mo was preferentially oxidized.

EXPERIMENTAL

ALLOY PREPARATION

Mo-Ni-Al alloys are known to exhibit a two phase (bcc Mo + β-NiAl) microstructure over a limited range of compositions. All the experiments in the present study were carried out in this phase field. Drop cast samples were prepared from pelletized elemental powder mixture of Mo (Alfa Aesar, 99.5% purity), Ni (MPC, 99.6% purity) and Al (Alfa Aesar, 99.8% purity) which

were arc-melted. The alloys were re-melted thrice to achieve a greater degree of homogenization followed by drop-casting in order to obtain a cylindrical rod. The composition was selected as $Mo_{20}Ni_{40}Al_{40}$ after studying the trends obtained from the cellular automata model described in the preceding section.

The Ni-Al-TM alloys were produced from pieces cut from pure bulk metal sheets obtained from the Materials Preparation Center at Ames Laboratory, having a purity of 99.7% or more. Pure Ni and Al were first arc-melted together in an argon atmosphere to form β-NiAl. The *ab-initio* calculations suggested that the transition metals have a preference for the Ni site in the *B2* structure. Alloys with compositions $Ni_{50-x}Al_{50}TM_x$, (x = 3, 6 and 9) were then arc-melted in an argon atmosphere. The samples were re-melted thrice to achieve better homogenization before drop-casting. The rods were annealed at 1300 °C in an argon atmosphere for 6 hours to ensure homogeneity. SEM was used to characterize the microstructure while phase analysis was done using x-ray diffraction (XRD) on a Philips PANalytical x-ray diffractometer (Panalytical, Almelo, Netherlands) with a Bragg-Brentano geometry and Cu $K\alpha_1$ radiation (λ = 1.54056 Å). The x-ray data was Rietveld refined using the GSAS software in order to estimate the lattice parameters of the phases as well as determine site preference for different elements [6]. Of the transition metals studied, it was observed that alloys with Platinum group metal (PGM) modifications formed single phase alloys while the other alloys showed a eutectic microstructure. Hence, further studies were carried out only on the PGM modified alloys. Hf additions are known to improve oxidation resistance of NiAl. Hence another set of alloys were prepared using Hf additions (0.05 atom%) to the PGM modified NiAl alloys.

OXIDATION TESTS

Mo-Ni-Al alloys were tested under isothermal conditions at 1100°C. Alloy coupons having 10mm diameter and 1mm thickness were oxidized in a open ended tube furnace for 20 hours. The mass change as a function of time was noted. The corresponding oxide scale was also studied using a JEOL 5910Lv scanning electron microscope. In case of the NiAl based alloys, isothermal oxidation at 1300°C was carried out in a Thermo Scientific Lindberg Blue M 1500 (Asheville, North Carolina) horizontal open tube furnace by passing dry air at a rate of 200 mL/min. The masses of the coupons were recorded before and after the oxidation test for each alloy. After each 100 hour test, the samples were removed from the furnace fore microstructural characterization. Each test was conducted twice for each of the alloys shown with the average being reported.

Cyclic oxidation at 1200 and 1300°C was manually carried out using a Thermo Scientific Lindberg Blue M 1500 (Asheville, North Carolina) horizontal open tube furnace. Each cycle consisted of two hours at the desired testing temperature followed by half an hour at ambient temperature at which time the mass measurements were recorded. The samples were removed from the furnace after one hundred hours at the testing temperature to characterize the scale microstructure.

After oxidation tests, each sample was gold sputtered and then copper plated. The copper coating helps to retain the oxide scale during the polishing process. After copper plating each sample was vertically mounted using epoxy resin. The samples were then cut so that the middle of the oxidized sample was visible at the surface. This surface was then polished on a polishing

wheel down to a 0.3μm surface finish. The polished samples were then analyzed using a JEOL 5910Lv scanning electron microscope (SEM) using an accelerating voltage of 20 kV.

GRAIN SIZE DETERMINATION

The grain size were determined using an AmRay 1845FE scanning electron microscope (SEM) utilizing an EDAX-TSL Delphi 2.5 Geneses model EBSD-EDX was used for orientation imaging microscopy (OIM). Epoxy mounted samples were polished according to standard metallurgical methods followed by electro-polishing for 8 seconds in a solution of 1 part 70% nitric acid 2 parts methanol at room temperature at 30 volts to remove smearing effects of mechanical polishing on the sample surface, as well as etch the alloy to bring out the grain boundary relief. The specimen was then lightly polished with colloidal silica to remove any adherent reaction products. The specimens were analyzed at a 70º from horizontal geometry. The resulting reflected Kikuchi patterns were analyzed using TSL version 5.02 software (TexSEM Laboratories, Inc. Draper, UT). A hexagonal pixel step pattern was used with step size small enough to assure at least 10 pixels per grain at a rate of 4 patterns per second. The resulting solutions and Hough filter solutions were recorded at each pixel for later evaluation. Average grain size was measured using the TSL software by estimating an ellipse to best fit each grain.

RESULTS AND DISCUSSION

OXIDATION OF Mo-Ni-Al ALLOYS

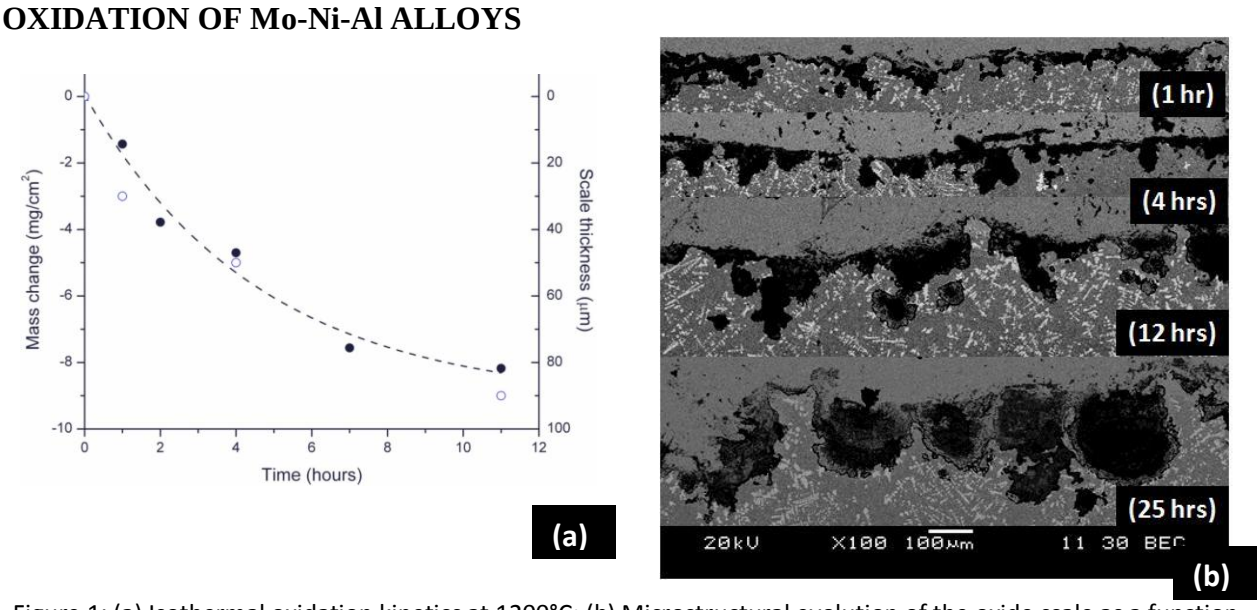

Figure 1: (a) Isothermal oxidation kinetics at 1200°C; (b) Microstructural evolution of the oxide scale as a function of time at 1200°C.

Figure 1(a) shows the kinetics of isothermal oxidation. Figure 1(b) shows the corresponding evolution of the oxide scale. These studies were carried out using coupons cut from the 10 mm diameter drop-cast alloy rods in the as-cast conditions. The SEM micrographs were taken roughly at the same relative position for each coupon (center of the coupon). The non-uniformity of the scale makes quantification a difficult problem. However, the thickness

averaged over multiple locations has been plotted alongside the mass change results in figure 1(a). By and large, this figure suggests a possibility of the mass change values converging into a steady state value. However, this was not conclusively observed during the current set of experiments. This trend can be understood better when one looks at the interface between the base alloy and the oxide scale. Alumina shows up in the back-scattered images as a very thin dark line, and usually forms just below the bright phase in the scale (MoO_2). At the end of 1 hour of oxidation, hardly any alumina seems to have formed. However, with increasing time, the amount of alumina increases steadily, until it covers a large area of the alloy. Therefore, despite the initial mass loss due to volatilization, indications are that the alumina will eventually seal the alloy surface.

The scale thickness increases in proportion to the mass change; this would be an expected result for alloys that gain mass on oxidation. In this case however, the fact that the scale thickens irrespective of the mass loss indicates that the mass change plots can be deceptive and the actual amount of Mo lost due to formation and subsequent volatilization of MoO_3 may actually be a little bit more than expected from the kinetics plot. The microstructures shown in figure 1(b) were taken from different coupons oxidized for different time durations. Hence it is difficult to map one on to the other; even then, it does appear suggestive that oxidation process proceeds by formation of initial "seeds" or regions of undulation that penetrate the alloy to a larger extent than the rest of the scale, and this is followed by "growth" or "coarsening" of these undulations with time.

ISOTHERMAL OXIDATION OF NiAl

Samples with varying levels of substitution for the Ni in β-NiAl base alloy were tested for oxidation resistance at 1300°C. The thermal shock at the end of the cycle could, in part, account for the spallation of the scale and therefore mass loss for some of the samples as shown in Table 1.

Alloy	Ni-50Al-**3X**	Ni-50Al-**6X**	Ni-50Al-**9X**
X=Pd	-1.58	-1.54	-1.55
X=Rh	-1.73	-1.08	1.42
X=Ir	-0.47	0.89	0.86

Table 1: Specific mass change (mg/cm^2) after isothermal oxidation at 1300°C for 24 hours
For reference, the baseline β-NiAl had a mass change of -1.75 mg/cm^2

As seen in Table 1, the palladium substitutions have negligible effect on the oxidation resistance of NiAl. Rh and Ir substitutions help improve the oxidation resistance, with higher substitutions leading to better oxidation resistance.

Figure 2 shows the oxide morphology of the oxidized samples containing 6 at% of each PGM after 24 hours of testing at 1300°C. The dark band between the copper plating and the sample is the oxide scale. Two of the images (Figure 2a and 2b) do not show this oxide scale, presumably because the oxide had spalled off, leaving behind new sample surface without a protective oxide.

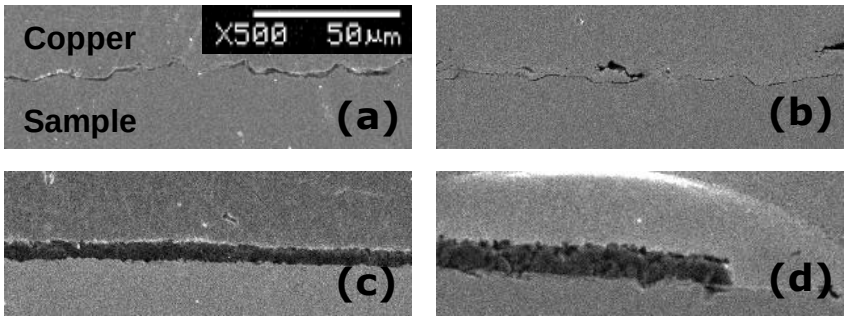

Figure 2: Microstructures of oxidized alloys after isothermal oxidation at 1300°C for 24 hours (a) β-NiAl, (b) Ni-50Al-6Pd, (c) Ni-50Al-6Ir, (d) Ni-50Al-6Rh

The oxidized microstructure of NiAl (Figure 2a) is almost identical to the oxidized microstructure of the Pd modified alloy (Figure 2b). As shown in the specific mass changes in Table 1, both of these alloys lost mass. These micrographs give evidence that the mass loss was due to the spallation of the oxide layer formed during oxidation testing. The oxide scale in the Rh modified alloy, while present, is not continuous (Figure 2d). The thickness of the remaining oxide was found to be about 10 µm. The Ir modified alloy shows a continuous oxide scale (Figure 2c), with a thickness of approximately 8 µm. Small amounts of hafnium additions to similar alloys have produced a more adherent and protective oxide scale[7]. Hence further tests were carried out by adding Hf in minor amounts to the Ni-50Al-6Rh alloy. Addition of as low as 0.05 at% Hf resulted in a mass gain of 0.46 mg/cm^2 while the same alloy without the Hf addition had a mass loss of 1.08 mg/cm^2 (See Table 1). Higher Hf additions showed similar mass gains, i.e. 0.1, 0.25, 0.5 at% Hf addition resulted in 0.47, 0.48, 0.54 mg/cm^{2}mass gain respectively. Hafnium addition was shown to result in forming an adherent and continuous oxide scale as shown in Figure 8 compared to discontinuous scale observed the same alloy without Hf addition (see Figure 2d). Therefore, the Hf additions were limited to 0.05 at% Hf for the alloys studied going forward.

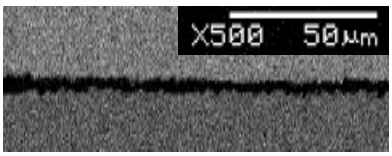

Figure 3: Microstructure of oxidized Ni-50Al-6Rh+0.05Hf alloy after isothermal oxidation at 1300°C for 24 hours

CYCLIC OXIDATION OF NiAl

Figure 4 shows the specific mass change curves for varying amounts of PGM substituted alloys. All of the 3% PGM alloys showed signs of spallation within the first few hours during this test. The 6% PGM substituted alloys all showed the effects of scale spallation within the first ten hours. The 9% PGM substituted alloys performed slightly better and did not show signs of spallation until after 20 hours. In the 6 and 9% PGM alloys it is noticed that the iridium containing alloy is the last to spall off its oxide scale. Both the palladium containing alloy along with the baseline β-NiAl showed poor oxidation resistance compared to the Ir and Rh substituted alloys. Again it can be seen that the hafnium along with the PGM substitutions give rise to the best oxidation resistant alloys. Of the PGM+Hf modified alloys, the PGM that gives rise to the most desired oxidation resistance is iridium. Cyclic oxidation results show a continuing trend that both iridium and to a lesser degree rhodium substitution to β-NiAl have a beneficial effect

on the oxidation resistance at high temperatures. Palladium additions continued to show little or no effect on oxidation when compared to the β-NiAl alloy. It is unknown at this time why palladium additions would have little effect on the scale adherence during cyclic oxidation while its neighbor on the periodic table, Rh, would have a significant effect. Grain size effects on oxidation of similar alloys have been noted previously. Other changes such as the thermal expansion coefficient could be playing a role here as well.

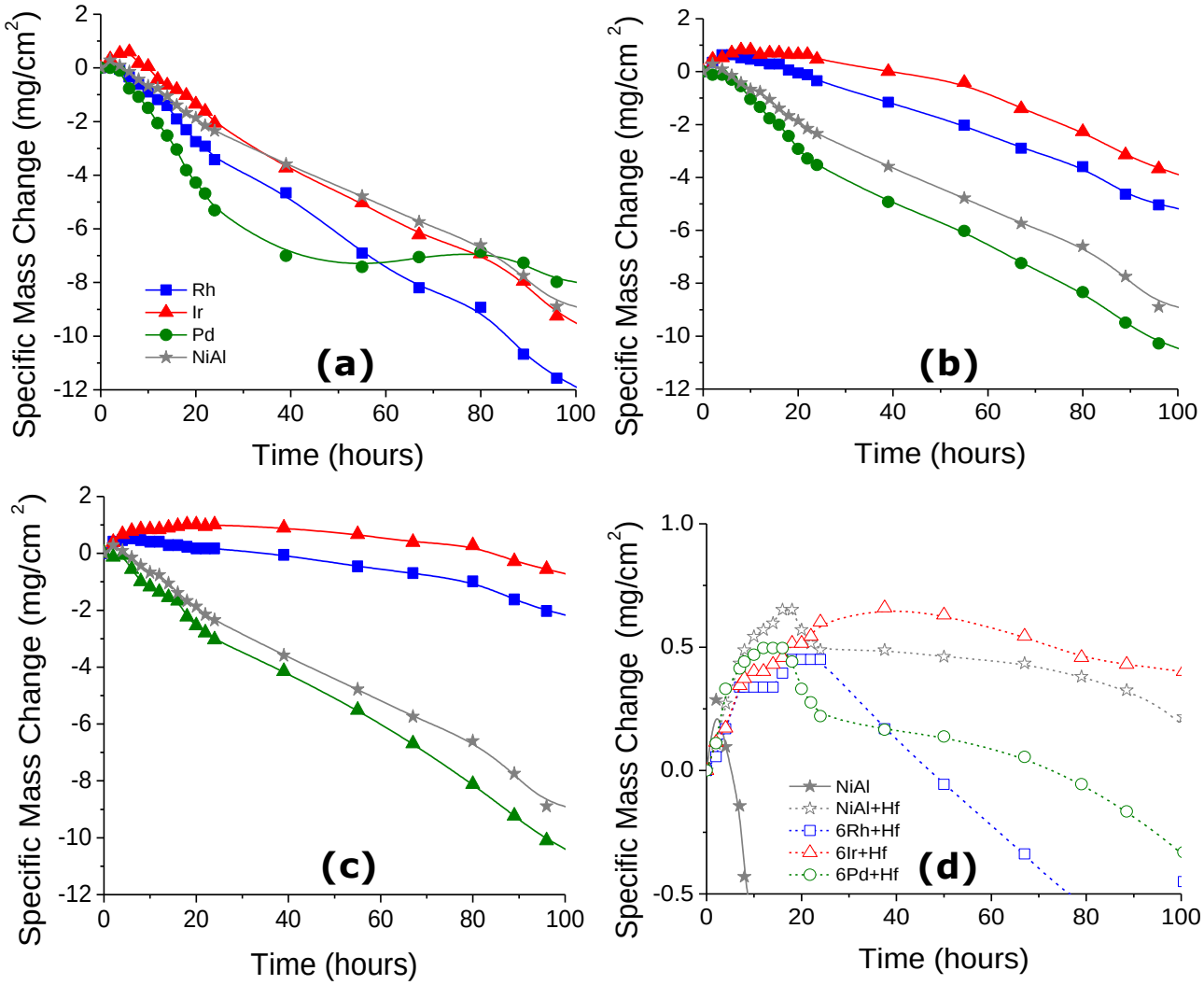

Figure 4: Mass change per surface area plots for alloys during cyclic oxidation at 1300°C for 100 hours (a) 3% PGM, (b) 6% PGM, (c) 9% PGM, (d) 6% PGM+Hf

The mechanism by which the improvement in oxidation resistance brought about by iridium, rhodium, and hafnium addition is unclear. In order to assess the role of Pd, Ir, and Rh substitution, the grain size of the PGM substituted cast and annealed samples were analyzed by OIM employing TSL software. The average grain sizes are displayed in Figure 5a. Figure 5b shows the role of Ir and Rh additions on the grain size the alloy on a finer scale. In Figure 5a, it can be seen that compared to the baseline NiAl, the palladium addition increases the average grain size at 3% but the grain size decreases with more Pd addition. For Ir and Rh, substitution

of these elements decreases the grain size. It seems Rh is more effective at lower concentrations than Ir but at the highest concentration of 9 at% Ir is more effective than Rh (120 vs. 160 µm).

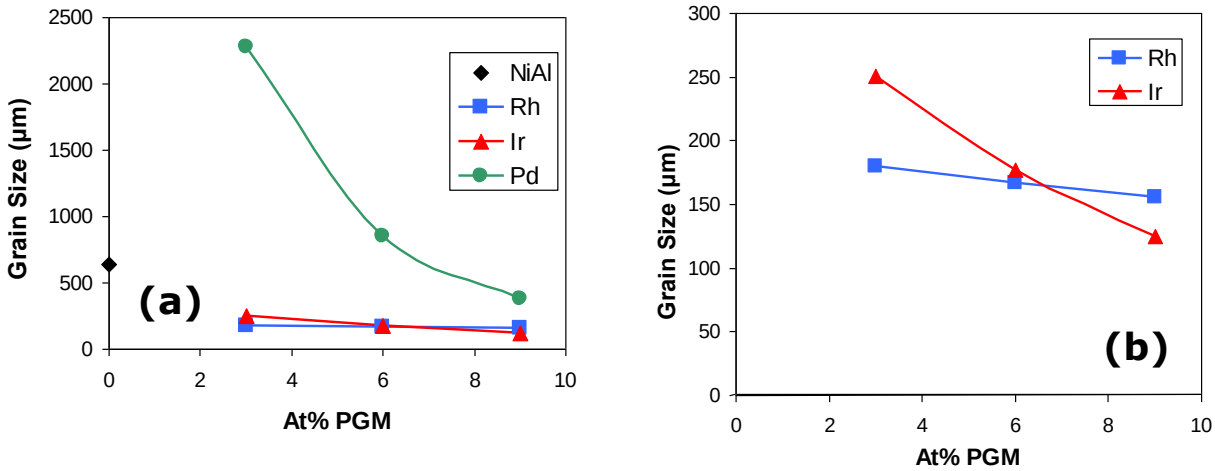

Figure 5: Average grain sizes for (a) NiAl and PGM modified alloys (b) Ir and Rh containing alloys

CONCLUSIONS

The Mo-Ni-Al showed a trend for forming a continuous alumina scale under isothermal conditions. However, a hermitic scale could form only after significant mass loss. Hence, it was deemed essential to develop an appropriate coating system. NiAl with Rh or Ir additions alongwith 0.05 atom% Hf showed excellent oxidation resistance and can be considered as a promising coating material, especially given the crystallographic match between the NiAl based coating and the base alloy. The superior oxidation resistance of NiAl based alloy can be attributed in part to the effect of Hf and the PGMs in reducing the grain size of the alloy.

REFERENCES

1. R.C. Reed, *The superalloys: Fundamentals and applications*. (Cambridge University Press, Cambridge, 2006).
2. J. H. Rose, John Ferrante, and John R. Smith, Physical Review Letters **47** (9), 675 (1981).
3. Chonghe Li, Joo Lim Hoe, and Ping Wu, Journal of Physics and Chemistry of Solids **64** (2), 201 (2003).
4. P. K. Ray, M. Akinc, and M. J. Kramer, Journal of Alloys and Compounds **489** (2), 357 (2010).
5. P.K. Ray, T. Brammer, Y.Y. Ye et al., JOM **62** (10), 25 (2010).
6. B.H. Toby, Journal of Applied Crystallography **34**, 210 (2001).
7. B. A. Pint, Surface and Coatings Technology **188-189**, 71 (2004).